Atmospheric Plasma-Assisted Deposition and Patterning of Natural Polymers

Artem Arkhangelskiy,* Alberto Quaranta,* Antonella Motta, Yuejiao Yang, Vamsi K. Yadavalli, and Devid Maniglio

Plasma-assisted deposition is a facile, yet sophisticated method to form biocompatible coatings on materials and introduce specific surface interactions. The plasma process provides unique features such as surface activation, functionalization, and assisted polymerization, all of which can be obtained under low power and room temperature conditions. Plasma-assisted deposition can further provide coatings with enhanced adhesion and stability. Here, it is reported for the first time, a method for the controlled plasma deposition of the versatile biomaterial chitosan on a range of substrates – soda-lime glass, metal alloy (Ti4Al6V), thermoplastic polymer (polyethylene terephthalate), and silicone rubber (poly(dimethylsiloxane)). The deposited chitosan films are characterized by atomic force microscopy, scanning electron microscopy and Fourier transform infrared spectroscopy, and evaluated for adhesion and stability. The proposed method is also successfully optimized for the deposition of multiple layers of different biomaterials. Specifically, coatings comprising alternate chitosan and silk fibroin layers are realized, together with patterned surfaces with programmable surface composition. The biological response of the chitosan-on-fibroin and fibroin-on-chitosan surfaces with and without patterning are investigated using cell culture experiments. Selective area deposition enables the development of improved surface finishes for biomedical devices.

1. Introduction

Polymeric coatings capable of guiding cell behavior and morphology have attracted increasing attention in recent years. Coating properties including surface morphology, topography, and chemistry are known to significantly affect cell adhesion, orientation, guidance, differentiation, proliferation, and gene expression.[1–4] Such coatings have also found effective applications in biosensors, biochips, drug delivery devices, prostheses, and implants. A diverse set of biocompatible polymers from synthetic and natural origin may be used. Despite advantages of synthetic polymers in terms of processing, stability, and mechanical properties, natural polymers are preferable for many applications due to their bioactivity, biodegradability, and biocompatibility.[5–6] Among natural polymers, chitosan, a linear polysaccharide derived from chitin, has been extensively investigated for biomedical, environmental, and food applications due to remarkable properties such as nontoxicity,[7] biodegradability,[8] antibacterial activity,[9] biocompatibility,[10] and immunological activity.[11] Moreover, due to chitosan's processability it can be designed into constructs including films,[12] membranes,[13] micro/nanofibers,[14] bandages,[15] micro/nanoparticles,[16] and hydrogels.[17]

Numerous techniques have been reported for the formation of chitosan coatings on different surfaces.[18] These are based on adsorption processes,[19–21] including methods such as dip-coating,[22] spin-coating,[23] layer-by-layer (LbL) deposition[24] and spray coating.[25] For short-term applications such as drug delivery, deposition of chitosan is based on electrostatic, Van der Waals, and hydrogen-bond interactions. Deposition methods based on covalent bonding are preferred for long-term applications such as coatings for implants and prostheses.[26–27] The deposition of chitosan generally consists of two steps – surface modification/activation (pre-treatment), followed by immobilization of the coating. Pre-treatment methods can involve physical modification, such as blasting and mechanical polishing, or chemical modification to introduce specific functional groups and change surface behavior (e.g., hydrophilicity, morphology, charge). Typically, these methods have disadvantages including low quality and limited control of the properties of the coating, together with low adhesion to the underlying surface. To solve

A. Arkhangelskiy, A. Motta, Y. Yang, D. Maniglio
BIOtech Center for Biomedical Technologies
Department of Industrial Engineering
University of Trento
Via Sommarive 9, Trento, TN 38123, Italy
E-mail: artem.arkhangelskiy@unitn.it
A. Quaranta
Department of Industrial Engineering
University of Trento
Via Sommarive 9, Trento, TN 38123, Italy
E-mail: alberto.quaranta@unitn.it
V. K. Yadavalli
Department of Chemical and Life Science Engineering
Virginia Commonwealth University
601 W Main Street, Richmond, VA 23284, USA

the problem of poor adhesion and to improve the initial properties of the coatings, pre-treatment[28–29] and post-treatment[30] methods are often required, impacting the time and costs of production. Potential alternatives are electrospray[31] and electrophoresis,[32] which provide fast and controlled deposition with relatively high adhesion strength on surfaces with complex shapes. Conversely, they are dependent on suspension parameters and cannot be applied on non-conductive substrates. Other techniques, such as electron beam sputtering depositing[33] can be also used, albeit limited by small deposition areas, thin coatings, and the need for high vacuum equipment. Cold plasma treatment provides a versatile and effective functionalization method by eliminating the use of hazardous solvents and chemical reagents.[18]

To enable coating of chitosan or other natural polymers for applications such as biosensors or implantable devices, the deposition method should provide not only a homogeneous and stable layer, but also provide spatially controlled deposition, potentially enabling surface patterning at the micro or nanoscales.[34–36] When the coatings interface with living environments, spatially-controlled deposition can tune interactions (e.g., protein adsorption), or guide cell organization. One method of pattering chitosan is based on the use of a pipette tip,[37] which allows contourable patterns. Hover, there are issues of low resolution and deposition on complex shapes, such as screws and non-planar implants. Similar issues are noted with other techniques such as photolithography[38] and inkjet printing deposition.[39] Most deposition methods can create coatings made of only a single material, or change the bioactivity only where the coating was assembled or patterned. Typically, implants integrated in human body are in contact with several types of tissues. For example, dental implants are in contact with trabecular bone, cortical bone and gingival tissue,[40–41] necessitating specific surface/tissue interactions. The combination of spatially controlled deposition, even on complex shapes, together with the possibility of depositing different biomaterials under mild conditions can allow for multifunctional controlled release coatings that can preserve the biological activity of therapeutic agents, coat multiple substrates of different length scales, and exhibit tuned, targeted, and/or responsive behaviors.[42] Moreover, the development of multiple stacked structures opens possibilities to produce complex sensor architectures with better performance.

Here, we present a novel approach for the deposition and patterning of chitosan via atmospheric plasma deposition. This method provides a controlled, room temperature deposition of chitosan on a wide range of materials such as glass, Ti6Al4V alloy, polyethylene terephthalate (PET), and poly(dimethylsiloxane) (PDMS). These substrates differ in characteristics (i.e., conductivity or flexibility). The structure of the deposited chitosan films was analyzed using attenuated total reflectance-Fourier transform infrared spectroscopy (ATR-FTIR), while the conformation and morphology of the coatings were studied by atomic force microscopy (AFM) and scanning electron microscopy (SEM). The stability of the chitosan coating was also assessed. This technique also allows the formation of patterns and the sequential deposition of two and more materials using a layer-by-layer (LbL) approach. To assess this, we showed the deposition of a second biopolymer, silk fibroin, whose plasma deposition was previously reported.[43]

Fibroin is one of the most interesting protein-based biomaterials,[44] often investigated as a complementary material for chitosan.[45–47] Indeed, fibroin and chitosan share similar deposition pathways (e.g., photolithography[48–49] and inkjet printing[50]). Representing a one-step technique without the need for pre-treatment, plasma-assisted deposition can provide a spatially controlled deposition, forming chitosan on fibroin (CoF), and fibroin on chitosan (FoC) films as well as patterned surfaces. We finally demonstrate their ability to tune cell adhesion and proliferation. Silk fibroin and chitosan coatings (F and C) were tested and compared with silk fibroin pattern on chitosan (*p*-FoC) and chitosan pattern on silk fibroin (*p*-CoF) samples. Chitosan fully coated with silk fibroin (FoC) and silk fibroin fully coated with chitosan (CoF) samples were also tested to understand the influence of coating thickness and the underlying layer. Patterned samples (silk fibroin patterns on silk fibroin (*p*-FoF) and chitosan patterns on chitosan (*p*-CoC)) were also compared with F and C samples. Plasma deposition is therefore presented as a versatile technique for biomaterial deposition for modifying the surfaces of devices and implants.

2. Results and Discussion

2.1. Atmospheric Plasma Deposition

Plasma deposition is a complex process that affects surfaces in terms of functionalization, sterilization, and etching, as well as the material inside the plasma tube by modification.[43] Plasma polymerization/deposition allows the formation of thin and homogeneous layers of different materials with strong adhesion to underlying surfaces.[51–53] Formed covalent bonds between functionalized substrate and deposited material enhance adhesion, preventing delamination.[54–57] The effect of the plasma on the structure of the chitosan has been widely investigated. During deposition, the plasma generates various excited species, free electrons, and radicals, such as OH•, H•, and O•. These reactive species interact with chitosan and promote cleavage of β-1-4 glycosidic linkages, oxidation of d-glucopyranose ring, generation of aldehyde groups, and dehydration at primary hydroxyl groups, leading to fragmentation of the main chains of chitosan.[58–59] During deposition, due to the use of argon and nitrogen as working and cooling gases, dehydration of the structure also occurs. Together, these factors promote chitosan crosslinking via hydrogen bonding between the aldehyde and amino groups.[60] In this work, the chitosan deposition and crosslinking are demonstrated on four different surfaces – glass, Ti6Al4V, PET, and PDMS. These surfaces not only have different chemistries, but also represent a diversity of shapes for the chitosan deposition.

2.2. Microstructure of Chitosan Coatings

Chitosan coatings on glass, PDMS, PET, and Ti6Al4V alloy are presented in **Figure 1**. The surfaces range from flat and rigid, to flexible and non-planar. The coatings have a uniform structure across all substrates, and the possibility of obtaining pattering structures by plasma-assisted deposition on non-planar surfaces is confirmed in Figure 1d. The plasma is electrically conductive
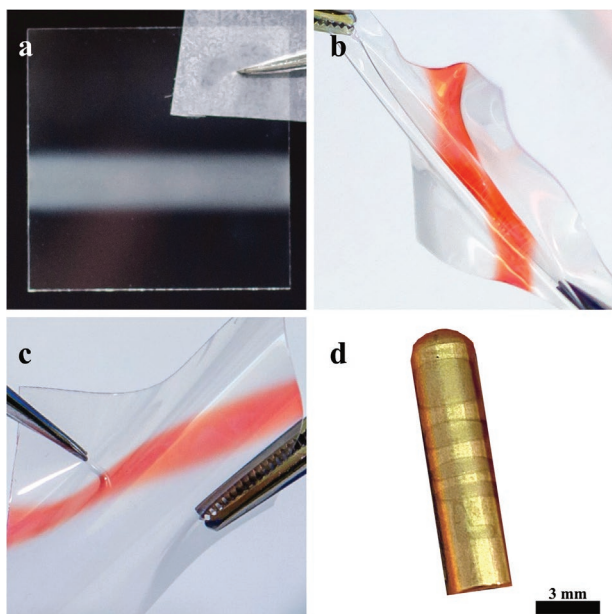
Figure 1. Images of coated samples on a) glass, b) PDMS, c) PET, d) Ti6Al4V cylindrical pins with patterned coatings. The red color is due to staining using Congo Red.

due to the presence of free electrons and behaves differently depending on the type of substrate – conductive or non-conductive. Depending on the physical properties, the surface of the substrate can be more or less impacted by plasma in terms of etching, roughening, and penetration of a deposited material. The influence of the surface on the conformation of chitosan coatings was investigated by means of atomic force microscopy (AFM). The nanoscale surface morphologies are presented in Figure S1, Supporting Information. Surface roughness (R_a) values measured on Ti6Al4V alloy, glass, PET, and PDMS are shown in **Table 1**.

The highest value of R_a was observed in the Ti6Al4V alloy sample (Figure S1d, Supporting Information). This is likely because the surface of the uncoated Ti6Al4V alloy substrate is machine polished and not uniform at the nanoscale. In the red square area (25×25 µm), the R_a is 122 ± 29 nm as the polished surface was significantly smoother. These values are compatible with the surface roughness range of 100–200 nm obtained by dip-coating.[61] Chitosan coating on glass also shows high values of R_a (Figure S1a, Supporting Information). It is notable that a similar morphology was reported earlier using photocrosslinkable chitosan,[62] while smaller roughness values of ≈1 nm were obtained using drop casting[63] and dip coating.[64] The chitosan coating on the PDMS substrate has the lowest surface

Table 1. Surface roughness values of deposited chitosan films on different surfaces. Roughness data was collected on 3 samples at 3 different spots ($n = 9$) on each sample.

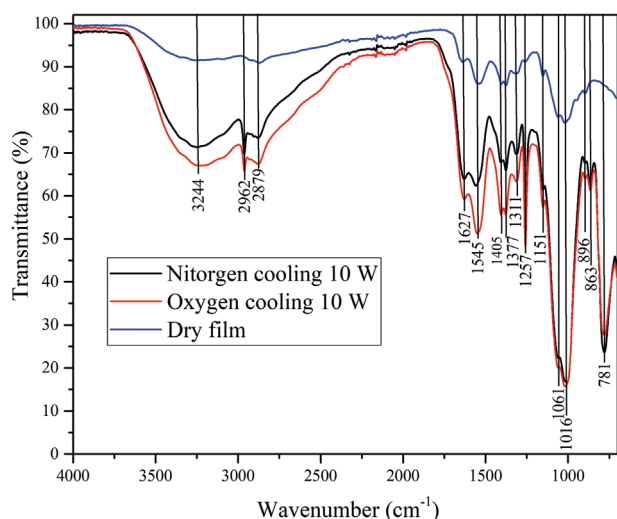| Substrate	Surface roughness (nm, mean ± SD)
Ti6Al4V alloy	260 ± 62
Glass	160 ± 31
PET	138 ± 33
PDMS	79 ± 12
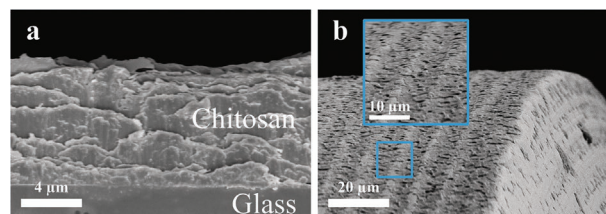
Figure 2. SEM images showing the cross-section of deposited chitosan on a) glass and b) a Ti6Al4V alloy screw.

roughness (79 ± 12 nm, Figure S1b, Supporting Information). Similar surface morphology was reported[65–66] with roughness values ≈1 nm using water-based deposition. The surface roughness of the chitosan coating on PET substrate is 138 nm $\pm$ 33 nm (Figure S1c, Supporting Information). Interestingly, the surface roughness is considerably higher than previously published,[29] where plasma pretreatment was employed. Thus, the plasma pre-treatment provides surface modification and increases the roughness of the substrate, without significantly impacting the underlying layers in terms of etching.

The surface morphology of the plasma deposited chitosan can be influenced by the presence of undissolved chitosan supramolecular assemblies that are present in the solution. The chitosan powder was dissolved in a weak 2% acetic acid solution without filtration, resulting in ≈1% of insoluble matter (w/w). Further sonication produced an aerosol solution with some insoluble fraction, which then was injected into a plasma torch gas line. Moreover, it is possible that the plasma region inside the torch could induce crosslinking reactions, promoting the growth of insolubility just before being deposited. It can also be supposed that difference in surface energy (λ_c) may have impact on the conformation of chitosan films. PDMS is a material with the lowest λ_c in the range of 15–20 mJ m^{-2}, which promotes lower R_a. Conversely, PET and Ti6Al4V alloy substrates, having higher λ_c, 30–40 mJ m^{-2} and 40–50 mJ m^{-2}, respectively, might result in the increase of R_a. Glass substrates with the highest surface energy values (about 300 mJ m^{-2}) can promote this process, resulting in the highest surface roughness. Importantly, the chitosan coatings have similar morphology on all substrates at the macroscale. Cracks are observed on PDMS substrates due to the difference in stiffness of chitosan and the underlying PDMS. It is worth mentioning that no cracks accrued on PET samples, enabling the coatings to be used in flexible devices. Figure S2, Supporting Information, shows SEM images of the coated and uncoated Ti6Al4V alloy screw confirming the deposition. The presence of undissolved chitosan is visible in the SEM cross-section image (**Figure 2**a). The surface morphology is confirmed by the SEM image of the screw surface (Figure 2b). In multiple deposition passes, the thickness and roughness depend on the number of runs that follows the same trend observed for silk fibroin plasma deposition (Figure S3, Supporting Information).[43]

2.3. Structural Analysis

FTIR was used to understand the effect of the plasma on the structure of the deposited chitosan films. **Figure 3** shows the

**ADVANCED
SCIENCE NEWS**
www.advancedsciencenews.com

**ADVANCED
MATERIALS
INTERFACES**
www.advmatinterfaces.de

Figure 3. ATR-FTIR spectra of plasma deposited chitosan films using nitrogen (black color) and oxygen (red color) cooling gases at 10 W power on PDMS substrate, and dry chitosan film produced by drop-casting of a stock solution (0.25% concentration) on a petri dish. To make plasma deposited films homogenous for the analysis the following deposition parameters were used: (17 runs – 2 runs at 100 mm min^{-1}, 5 runs at 300 mm min^{-1}, followed by 10 runs at 500 mm min^{-1}).

ATR-FTIR transmittance spectra of the dry chitosan film and the deposited chitosan films on PDMS substrates using different cooling gases at the same power (10 W), corresponding to the lowest power limit at which plasma can operate with reproducible stability.[43] The analysis of the FTIR peaks is presented in Table S1, Supporting Information.

As shown in Figure 3, the plasma has a minimal effect on the chemical structure of the biopolymer. Plasma-deposited and dry chitosan films exhibit the same intensity peaks at the same positions. The increased intensity of the absorption picks might be related to the crosslinked structure induced by the plasma reaction.[43,67] The chitosan film deposited using oxygen as the cooling gas has a slightly higher intensity in the areas from 3500 to 2000 cm^{-1} and from 1630 to 1500 cm^{-1} in comparison with the chitosan film deposited using nitrogen as the cooling gas. Changes in the range from 1630 to 1500 cm^{-1} are promoted by using compressed air cooling, with oxygen molecules tending to neutralize free electrons from the plasma. This makes it less physiochemically effective and slows the crosslinking reaction. Increasing the oxygen concentration in the cooling gas may increase the amount of oxygen-containing groups, such as C–O, C=O, and –COOH groups, as well as breaking and oxidation of the 1-4-glycosidic bonds, resulting in the fragmentation of the chitosan chains fragments with lower molecular weights.[68,59]

2.4. Stability and Adhesion of the Coatings in Aqueous Environments

In order to assess the quality of adhesion of the deposited chitosan to the underlying substrates, a peel test using adhesive tape (**Figure 4**a) and stability test in PBS buffer (Figure 4b) were performed. In comparison to plasma-deposited silk

fibroin films,[43] chitosan films show better adhesion to PDMS substrates. It is hypothesized that the outstanding adhesion is owing to chitosan's ability to link directly to the surface via various functional groups such as –COOH or –CHO.[18] In prior works on chitosan deposition using plasma pre-treatment modification on PET[29] and Ti alloy[69] substrates, improved adhesion was also reported. The adhesion results on Ti alloy can be compared to those obtained using electrophoretic deposition.[70] Images of the samples before and after soaking in phosphate-buffered saline (PBS) solution over 2 weeks are shown in Figure 4b. (additional images are presented in Figure S4, Supporting Information). As noted above, the plasma promotes crosslinking providing high film stability. A slight decrease in stability of the chitosan film on PDMS after sonication is presumably due to cracks that allow water to pass between the chitosan film and the PDMS substrate. We further assume that the deposited films are already relatively dry due to dehydration and the inert environment, allowing them to stay stable in air for significant periods of time without degradation. We also expect that the deposited chitosan coating will be degraded in vivo by enzymatic degradation to non-toxic components or in vitro by oxidation, chemical, or enzymatic hydrolysis, as reported in the literature[71]

2.5. Silk Fibroin and Chitosan Patterning

To evaluate the ability to deposit multiple materials on a single surface in a multilayer configuration, a glass slide was alternatively coated with silk fibroin and chitosan, resulting in three areas with different compositions (Figure S5a, Supporting Information). Prior to patterned deposition, the PDMS mask was gently attached to the glass slide, providing no air gap between the substrate and the mask. For samples in which chitosan was simply coated with silk fibroin, and silk fibroin coated with chitosan, we use the nomenclature (CoF) and (FoC) respectively. Patterned chitosan and silk fibroin substrates on the glass slides are presented in Figures S5b,c, Supporting Information. More complex geometries were also performed to mimic biosensor structures (Figures S5d–f, Supporting Information). LbL deposition was also conducted to understand the possibility of producing printed circuit board (PCB) configurations or to precisely tune surface properties. **Figure 5**a–c show SEM images of silk fibroin on chitosan (FoC) and chitosan on silk fibroin (CoF) in the form of layered structures. The images demonstrate the presence of silk fibroin and chitosan layers, and reveal that the chitosan has a less homogeneous structure in comparison to the fibroin. CoF surfaces (Figure 5d) show a slightly higher surface roughness (178 ± 26 nm), in comparison to chitosan coating on glass (160 ± 31 nm). This can be explained by the presence of the underlying layer of silk fibroin. On the other hand, FoC (Figure 5b) exhibits a smoother surface (116 ± 16 nm), with the silk fibroin filling in the chitosan underlying roughness and homogenizing the film (Figure S6, Supporting Information). The R_a of the silk fibroin coating on a glass is 45 ± 9 nm. The crack observed in SoC structure might result from the high thickness of the deposited layers and the fragile nature of chitosan.[72] Moreover, the deposited chitosan and silk fibroin films, even if dry, undergo an equilibration
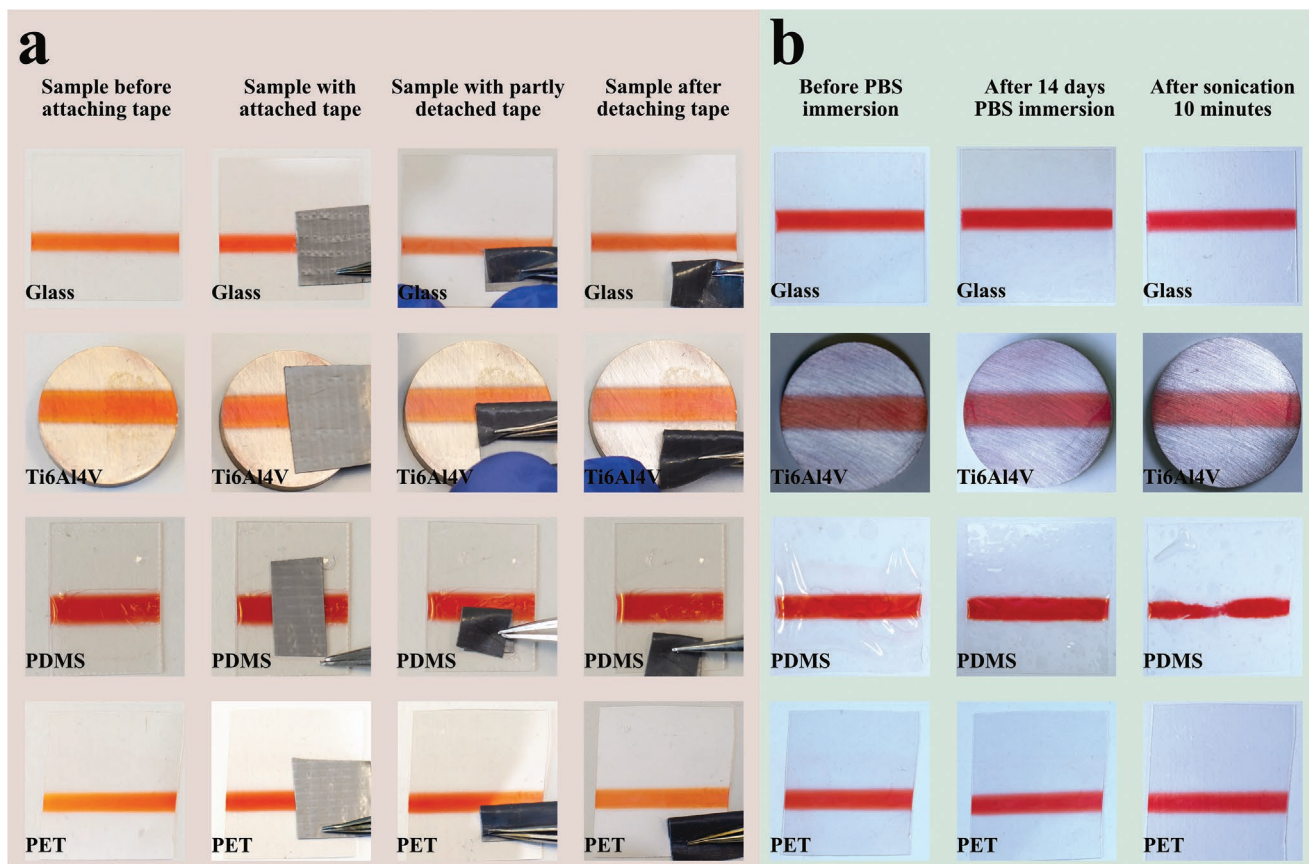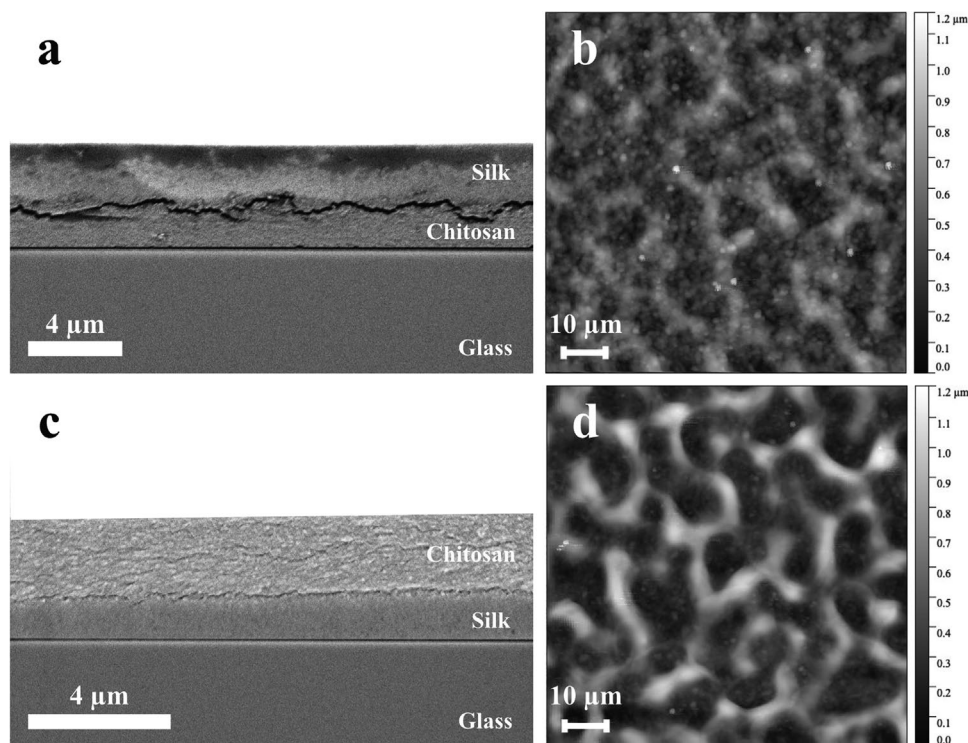
Figure 4. a) The chitosan film before and after a peel test using adhesive tape. Before testing, samples were immersed into Congo Red solution and dried with nitrogen. b) Chitosan films were observed in buffer solution for 2 weeks at 37 °C, followed by ultrasonication treatment in water. All images were obtained in dry condition.

of water content (6–8% in case of silk fibroin[73] and 7–11% in case of chitosan[74]), Such materials may also undergo dehydration inside SEM vacuum chamber, generating tensions between coating and stiff underlying support, leading to crack formation/delamination.

2.6. Cell Adhesion

To evaluate cell behavior on patterned and plasma LbL deposited coatings, human bone marrow-derived mesenchymal stem cells (hMSCs) were seeded directly on the surface with different coatings and cultured for 7 days in standard conditions (**Figure 6**). Detailed sample explanation is showed in **Table 3**. Patterned samples (silk fibroin patterns on silk fibroin (*p*-FoF) and chitosan patterns on chitosan (*p*-CoC)) were compared with F and C samples (Figures S15–S26, Supporting Information) and show no difference between these coatings. This proves that the surface morphology involved with patterns obtained from a single pass deposition does not affect cell adhesion, with an evident tendency of spreading (Figures S18–S20 and Figures S24–S26, Supporting Information). This behavior could be explained by coating inhomogeneities and/ or structural changes induced by plasma deposition. This can particularly be critical with silk fibroin, as reported earlier[75]

and with chitosan.[76] On Day 3 and Day 7, the cells were spread on the silk fibroin region and flat on the chitosan region, remaining in round shape or forming clusters. After 7 days culture, the cells on the silk fibroin regions significantly proliferated, forming a uniform layer. Due to strong contrast of cell adhesion behavior on silk fibroin and chitosan, the patterns made of the two materials were strongly visible in fluorescence after 7 days culture (Figure 6i–m), reproducing the behavior on uniform material coatings (Figure S15–S26, Supporting Information). It can be observed that on Day 7, the cells on the silk fibroin region in *p*-FoC sample show different morphology and have better spreading, while the cells on the silk fibroin regions in *p*-CoF, *p*-FoF and F samples form clusters. Silk fibroin structure can be easily affected by the underlaying structure, resulting on different materials properties and cell behaviors.[77–78] We assume that the silk fibroin regions of *p*-FoC and FoC have the same properties due to the similar production process, allowing us to use the FoC sample for further explanations of the silk fibroin regions of *p*-FoC sample. To evaluate this behavior, FTIR-ATR measurements were performed on three types of samples (F, FoC, and CoF) with glass as the substrate. To understand the structure of only the silk fibroin layer in the FoC sample and eliminate the influence of chitosan on absorption data, the measurement was also performed using chitosan on glass (C) as the background. Comparing the IR

**ADVANCED
SCIENCE NEWS**
www.advancedsciencenews.com

**ADVANCED
MATERIALS
INTERFACES**
www.advmatinterfaces.de

Figure 5. SEM images showing the cross-section and surface morphology of the multilayered structures on glass substrates. a) Cross-section of deposited silk fibroin on chitosan (FoC). b) Morphology of the FoC. c) Cross-section of deposited chitosan on silk fibroin (CoF). d) Morphology of the CoF. Each layer was deposited using 30 runs at 100 mm min^{-1}. Roughness data was collected on three samples at three different spots ($n = 9$) on each sample.

spectra and positions of absorption picks of silk homogeneous coating on glass (F) and silk firoin layer in the FoC sample, it is seen that both show a similar structure. It may be supposed that the chitosan was successfully eliminated from the measurements and both layers may be compared using secondary stucture deconvolution. These layers exibit the same secondary structure of Amide I peak (Figure S28b, Supporting Information), suggesting that the chitosan or glass underlayer does not affect the fibroin conformation. Other important factors influencing cell behavior are surface morphology and homogeneity of the layer.[79] The thickness and the roughness of the first (base) and the second layers were measured together with the contact angle and are shown in **Table 2**. We suggest that the deposited silk fibroin layer on the chitosan layer (p-FoC and FoC) can be heterogeneous (Figure S7 and Figure S8, Supporting Information). The chitosan layer of p-FoC and FoC has 248 ± 48 nm thickness with 41 ± 8 nm surface roughness, while thickness on the deposited silk fibroin layer is approximately 69 ± 49 nm. We expect that when the thickness of the deposited silk fibroin layer is ≈20 nm, local inhomogeneities are formed. This hypothesis is supported by the contact angle data (Figure S27, Supporting Information and Table 2). Silk fibroin coating on glass (F) has slightly hydrophobic properties with the contact angle at 93° ± 3° (Figure S27a, Supporting Information), while the chitosan coating on glass (C) has hydrophilic character (contact angle 49° ± 1°, Figure S27c, Supporting Information). A reduction of the contact angle of FoC sample to 54° ± 4° (Figure S27b, Supporting Information) is observed, which might be due to uncovered chitosan. The CoF sample exhibits same hydrophilic behavior (contact angle

56° ± 2°) (Figure S27d, Supporting Information) as chitosan due to low influence of silk fibroin underlying layer. F and FoC samples show approximately the same surface roughness – 41 nm ± 8 nm and 54 nm ± 9 nm, respectively, suggesting that cell behavior and contact angle are mostly affected by different surface chemistry. It is also likely that the presence of silk fibroin can slightly increase the cell interaction of chitosan (Figure 6k–o).

3. Conclusion

We have demonstrated a one-step facile method for the deposition of chitosan via atmospheric plasma torch. This technique allows conformable chitosan coatings with excellent stability and strong adhesion to the underlying surfaces (Ti6Al4V alloy, PDMS, PET, glass) thanks both to plasma surface activation and plasma-assisted crosslinking. The deposited layers were characterized by ATR-FTIR, confirming that the plasma has minimal influence on the structure of chitosan, while the obtained morphology indicates the presence of undissolved supramolecular assemblies. The unique properties of the process, such as low power and dry deposition, enable layer-by-layer deposition, together with patterning of chitosan. Layering and patterning capability was then extended to conjugate chitosan to silk fibroin, checking the realization of controlled geometrical structures. The obtained patterns were then tested for cell adhesion and distribution. Cold plasma-assisted fibroin/chitosan patterns revealed the capacity of multilayers to control and guide cell behavior. This versatility can represent a powerful method for obtaining multifunctional
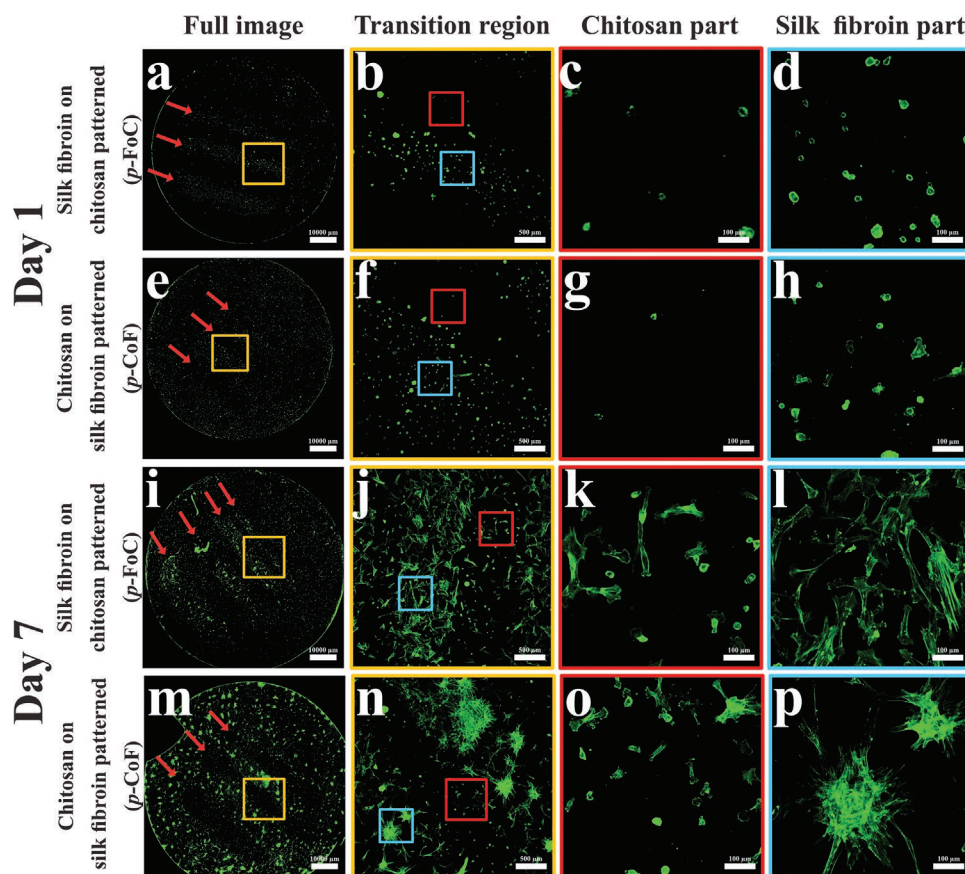
Figure 6. Cell culture test samples. a) Silk fibroin on chitosan patterned (*p*-FoC) Day 1 full. b) Silk fibroin on chitosan patterned (*p*-FoC) Day 1 transition region. c) Silk on chitosan patterned (*p*-FoC) Day 1 high magnification chitosan part. d) Silk fibroin on chitosan patterned (*p*-FoC) Day 1 high magnification silk part. e) Chitosan on silk fibroin patterned (*p*-CoF) Day 1 full. f) Chitosan on silk fibroin patterned (*p*-CoF) Day 1 transition region. g) Chitosan on silk fibroin patterned (*p*-CoF) Day 1 high magnification chitosan part. h) Chitosan on silk fibroin patterned (*p*-CoF) Day 1 high magnification silk part. i) Silk fibroin on chitosan patterned (*p*-FoC) Day 7 full. j) Silk fibroin on chitosan patterned (*p*-FoC) Day 7 transition region. k) Silk fibroin on chitosan patterned (*p*-FoC) Day 7 high magnification chitosan part. l) Silk fibroin on chitosan patterned (*p*-FoC) Day 7 high magnification silk part. m) Chitosan on silk fibroin patterned (*p*-CoF) Day 7 full. n) Chitosan on silk fibroin patterned (*p*-CoF) Day 7 transition region. o) Chitosan on silk fibroin patterned (*p*-CoF) Day 7 high magnification chitosan part. p) Chitosan on silk fibroin patterned (*p*-CoF) day 7 high magnification silk part.

surfaces suitable for applications in biomedical implants. The possibility to create multiple stacked structures can also enable the production of novel bioelectronic devices.

4. Experimental Section

Preparation of Chitosan Solution: chitosan solution 0.5% (m/v) was prepared by dissolving 0.1 grams of chitosan powder (Merck, Sigma-Aldrich) into 20 mL of 2% acetic acid aqueous solution followed by

steering at room temperature for 24 h. The solution was then diluted two times with deionized (DI) water to achieve a concentration of 0.25% in order to generate a stable aerosol solution, enabling continuous plasma deposition.
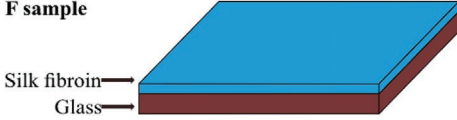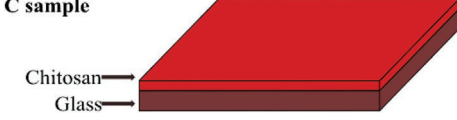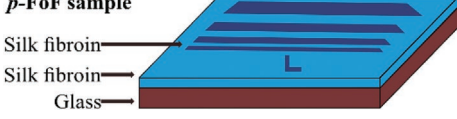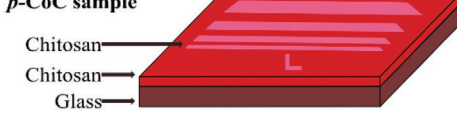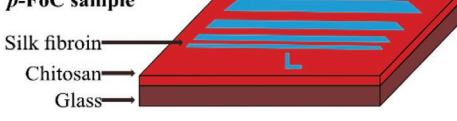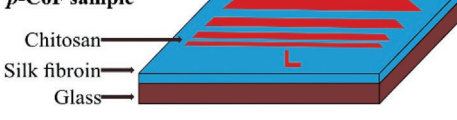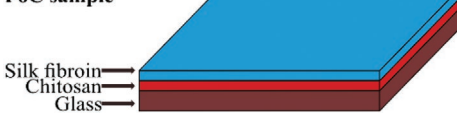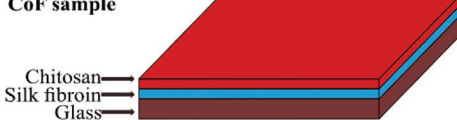
Preparation of silk-fibroin solution: B. mori silk cocoons (Chul Thai Silk Co., Phetchabun, Thailand) were cut into small pieces and then boiled two time for 90 minutes in an aqueous solution of Na_2CO_3 (Sigma-Aldrich), the concentration of the salt for first bath was set at 1.1 g L^{-1}, the second bath at 0.1 g L^{-1}, in order to remove glue-like sericin proteins, and then washed with distilled water and dried in air at room temperature overnight. The degummed silk fibroin was then

Table 2. Contact angle, thickness and roughness of deposited samples for cell culture and cell seeding tests. Thicknesses of the layers were measured by a separate deposition on glass slide and AFM analysis. Roughness data was collected on three samples at three different spots ($n = 9$) on each sample. Thickness data were collected by measuring height profile 5 times on two samples ($n = 10$). Contact angle was collected by measuring angle of 6 water drops ($n = 6$).

Sample	Water contact angle (°, mean ± SD)	Thickness (nm, mean ± SD)	Roughness (nm, mean ± SD)
Silk fibroin (F)	93 ± 3	160 ± 47	45 ± 6
Chitosan (C)	49 ± 1	248 ± 48	41 ± 8
Silk fibroin on chitosan (FoC)	54 ± 4	69 ± 49 (F layer)	54 ± 9
Chitosan on silk fibroin (CoF)	56 ± 2	56 ± 40 (C layer)	64 ± 8

Table 3. Sample configurations investigated and deposition information.

	CODE	Sample information	Note	Schematic images
1	F	Bare silk fibroin	Samples were prepared by 2 runs deposition of silk fibroin	**F sample** — Silk fibroin / Glass
2	C	Bare chitosan	Samples were prepared by 2 runs deposition of chitosan	**C sample** — Chitosan / Glass
3	p-FoF	Silk fibroin on silk fibroin patterned	Samples were prepared by 2 runs deposition of silk fibroin and 1 run patterned deposition of silk fibroin	**p-FoF sample** — Silk fibroin / Silk fibroin / Glass
4	p-CoC	Chitosan on chitosan patterned	Samples were prepared by 2 runs deposition of chitosan and 1 run patterned deposition of chitosan	**p-CoC sample** — Chitosan / Chitosan / Glass
5	p-FoC	Silk fibroin on chitosan patterned	Samples were prepared by 2 runs deposition of chitosan and 1 run patterned deposition of silk fibroin	**p-FoC sample** — Silk fibroin / Chitosan / Glass
6	p-CoF	Chitosan on silk fibroin patterned	Samples were prepared by 2 runs deposition of silk fibroin and 1 run patterned deposition of chitosan	**p-CoF sample** — Chitosan / Silk fibroin / Glass
7	FoC	Silk fibroin on chitosan	For section 2.5 samples were prepared by 30 runs deposition of chitosan and 30 runs deposition of silk fibroin. For the sections 2.6 and 2.7 samples were prepared by 2 runs deposition of chitosan and 1 run deposition of silk fibroin	**FoC sample** — Silk fibroin / Chitosan / Glass
8	CoF	Chitosan on silk fibroin	For section 2.5 samples were prepared by 30 runs deposition of silk and 30 runs deposition of chitosan. For the sections 2.6 and 2.7 samples were prepared by 2 runs deposition of silk fibroin and 1 run deposition of chitosan	**CoF sample** — Chitosan / Silk fibroin / Glass

dissolved in 9.3 M LiBr solution for 4 h at 65 °C. The produced silk fibroin LiBr solution was dialyzed against deionized water using a dialysis cassette (MWCO 3500, Pierce, 0.5–3 ml) at room temperature for 3 days to remove the salt, followed by filtering with a glass filter in order to remove silk aggregates and moisture.[80] The concentration of silk fibroin solution was evaluated by measuring the absorbance at 280 nm (Nanodrop, ThermoFisher), and was about 5–5.5% (w/v) and then was diluted to 0.25 wt.% by adding deionized water, adjusted minimize plasma torch breakage and enable stable plasma deposition.

Plasma Torch: plasma-assisted deposition of chitosan and silk fibroin aerosol solution was conducted using an atmospheric plasma torch (Stylus Plasma Noble, Nadir Tech SR[81]). The torch consists of a radiofrequency (RF) generator, a high voltage (HV) generator and a gas carrier system. The ignition and extraction of the plasma flow is provided by an HV generator. The adjustment of the plasma plume and plasma parameters are controlled by the user through the RF generator and an impedance matching circuit. The gas system provides a controlled gas supply and consists of three channels: the working channel for ignition of the plasma, the cooling channel for reducing the temperature of the system, and the injection channel for the delivery of aerosol precursors into the plasma region.

Plasma Deposition of Chitosan and Silk Fibroin: Ddeposition was conducted using a previously described method.[43] Briefly, aerosol solutions were obtained by ultrasonication of the silk fibroin or chitosan stock solutions, which were injected into the plasma torch gas line and oriented towards the chosen substrates (glass, PET, PDMS, and Ti6Al4V alloy). The substrates were placed on a three-axis motorized stage. The plasma power was set at 10W, distance between the plasma torch and the substrate was ≈6 mm, the torch speed was set to 100 mm min^{-1}, 300 mm min^{-1}, and 500 mm min^{-1}. The plasma was ignited using pure Ar at a flow rate of 5 standard liters per minute (slm). N$_2$ or compressed air (15 slm flow rate) were utilized as cooling gases, while Ar (0.3 slm) was used for the delivery of aerosol precursors. Deposition on planar surfaces were made either via linear or square deposition, while deposition on a cylindrical geometry (Ti6Al4V alloy cylindrical pin and Ti6Al4V alloy dental screw (Lincotek Trento S.p.A))

**ADVANCED
SCIENCE NEWS**

www.advancedsciencenews.com

**ADVANCED
MATERIALS
INTERFACES**

www.advmatinterfaces.de

were made by putting the samples in rotation by means of a stepper motor. In linear deposition, one run was set as a path through the entire samples. In the case of square deposition, the pathway is presented in Figure S29a, Supporting Information, and was set as 1 run. Patterning of silk fibroin and chitosan was made by using a PDMS mask (Figure S29b, Supporting Information), attached to the samples before the deposition and then gently detached after. For protein absorption, electrophoresis and cell culture and cell seeding tests samples were prepared as follows. Glass slides 15 mm in diameter were put in pure ethanol and sonicated for 30 min, followed by washing with acetone, then washed with pure ethanol, rinsed in DI water and then dried under nitrogen flow. 8 types of samples were prepared – silk fibroin (F) and just chitosan (C) samples; silk fibroin patterning on silk fibroin (*p*-FoF) and chitosan patterning on chitosan (*p*-CoC); silk fibroin patterning on chitosan (*p*-FoC) and chitosan patterning on silk fibroin (*p*-CoF); silk fibroin on chitosan (FoC) and chitosan on silk fibroin (CoF). Different samples information is listed in Table 3. Schematic images of each sample are presented in Figure S30, Supporting Information. Prior to all the tests (protein absorption test, electrophoresis cell culture, and cell seeding tests), the samples were sterilized by soaking into 75% ethanol for 30 min and followed by rinsing three times in DI water to remove ethanol.

Cell Culture and Cell Seeding: human bone marrow-derived mesenchymal stem cells (hMSCs) were used in this study. The cells were cultured in the Dulbecco's Modified Eagle Medium/Nutrient Mixture F-12 (DMEM/F-12) with 10% fetal bovine serum (FBS), and 1% antibiotic/antimycotic. The cells were cultured in a T75 flask at 37 C with 5% CO2 in a humidified atmosphere. The cells were fed every two days until the cells reached 70% confluence. The cells (at passage 2) were detached from the flask by 1% trypsin-EDTA solution, re-suspended in standard medium, and were seeded directly on the samples in a 24-well plate (20000 cells per well in 0.4 ml medium). The medium was changed every two days.

Confocal image analysis: cell adhesion was visualized by Oregon green phalloidin and 4′6-diamidino-2-phenylindole (DAPI) staining. Oregon green phalloidin stains cytoskeleton resulting in green fluorescence while DAPI stains nuclei resulting in blue fluorescence. At each time point, the cell-seeded samples were fixed with 4% paraformaldehyde for 30 min, washed three times with PBS (15 minutes each time), and then were permeabilized using 0.1% Triton X-100 PBS solution for 30 min. After washing in PBS for 3 times (15 minutes each time), cells were incubated with Oregon green phalloidin (5.0 µl per sample) and DAPI (1.0 ml per well, 5.4 µl dilute in 25.0 ml PBS) for 45 min at room temperature. After three rinses with PBS, samples were observed by confocal microscopy (Nikon – A1, USA).

Physical and Chemical Characterization: photos of the samples were made using a digital camera Canon 650D. In order to make the chitosan films visible, they were immersed in 10^{-4} M congo red aqueous solution for 5 min, while the silk fibroin films were immersed in 2% crystal violet solution for 5 minutes. High-resolution electron micrographs were obtained using a Supra 40 (Zeiss, Germany) field emission electron microscope (FESEM). Samples were coated with 4 nm Pt80/Pd20 alloy by plasma sputtering. Surface topography was collected using an atomic force microscope (NT-MDT Solver Pro, Russia) in semi-contact mode. Surface roughness (R_a) values have been calculated using Gwyddion software. For each sample, the area of observation was 88.8×88.8 µm, which is the maximum area provided by the equipment. The image of the edge of the silk fibroin film was obtained by applying a thin PDMS mask on the substrate to control deposition. The top and bottom plane were fitted using Gwyddion software to calculate the profile. FTIR was performed in the range 400–3800 cm^{-1} with a Nicolet Avatar 330. FTIR spectra were collected in ATR mode, mediating 32 scans with a resolution of 2 cm^{-1}. Deconvolution of the amide I spectra (1590–1710 cm^{-1}) was used to analyze the secondary structure of silk fibroin films.[82–83] Peak position detection was done using a Fourier self-deconvolution technique.[84] Gaussian function was used to fit the peaks in order to reduce χ^2. The different secondary structures (random coil, beta-sheets, turns, α-helix, and side chains) were obtained from the calculation of the area of each peak. Contact angle analysis were performed at a constant temperature of 22 °C by releasing a water drop of 5 µm. With the help of ImageJ software the contact angle of the droplets was calculated. Physical stability of chitosan films was evaluated by putting samples in PBS solution (pH 7.4) for 2 weeks at 37 °C, followed by treatment in sonication bath for 10 min. Adhesion strength was evaluated by a peeling test using adhesive tape (LUX Gewebeband Universal).

Statistical Analysis: Data are shown as mean±SD. Roughness data was collected on three samples at three different spots ($n = 9$) on each sample. Thickness data were collected by measuring height profile 5 times on two samples ($n = 10$). Contact angle was collected by measuring the angle of six water drops ($n = 6$). Mean values and standard deviation then were calculated.

Supporting Information

Acknowledgements

Conflict of Interest

The authors declare no conflict of interest.

Data Availability Statement

The data that support the findings of this study are available from the corresponding author upon reasonable request.

Keywords

[1] S. Cai, C. Wu, W. Yang, W. Liang, H. Yu, L. Liu, *Nanotechnol. Rev.* **2020**, *9*, 971.

[2] D. Kołbuk, M. Ciechomska, O. Jeznach, Sajkiewicz, *RSC Adv.* **2022**, *12*, 4016.

[3] D. Kourti, A. Kanioura, M. Chatzichristidi, K. G. Beltsios, S. E. Kakabakos, S. Petrou, *Eur. Polym. J.* **2022**, *162*,, 110896.

[4] S. Samanta, D. Gaad, A. Cabet, A. Lilienbaum, A. Singh, D. K. Aswal, M. M. Chehimi, *Surfaces* **2021**, *4*, 306.

[5] S. Pradhan, A. K. Brooks, V. K. Yadavalli, *Mater. Today Bio* **2020**, *7*, 100065.

[6] M. S. B. Reddy, D. Ponnamma, R. Choudhary, K. K. Sadasivuni, *Polymers (Basel)* **2021**, *13*, 1105.

[7] A. Ali, S. Ahmed, *Int. J. Biol. Macromol.* **2018**, *109*, 273.

[8] S. Ahmed, S. Ikram, *Achiev. Life Sci.* **2016**, *10*, 27.

[9] M. Wu, Z. Long, H. Xiao, C. Dong, *Carbohydr. Res.* **2016**, *434*, 27.

[10] A. Babu, R. Ramesh, *Mar. Drugs* **2017**, *15*, 96.

[11] N. M. Alves, J. F. Mano, *Int. J. Biol. Macromol.* **2008**, *43*, 401.

[12] A. De Masi, I. Tonazzini, C. Masciullo, R. Mezzena, F. Chiellini, D. Puppi, M. Cecchini, *Biophys. Rev.* **2019**, *11*, 807.

[13] L. Cui, S. Gao, X. Song, L. Huang, H. Dong, J. Liu, F. Chen, S. Yu, *RSC Adv.* **2018**, *8*, 28433.

[14] N. D. Al-Jbour, M. D. Beg, J. Gimbun, A. K. M. M. Alam, *Curr. Drug Delivery* **2019**, *16*, 272.

[15] M. Burkatovskaya, G. P. Tegos, E. Swietlik, T. N. Demidova, A. P Castano, M. R. Hamblin, *Biomaterials* **2006**, *27*, 4157.

[16] N. Islam, I. Dmour, M. O. Taha, *Heliyon* **2019**, *5*, e01684.

[17] P. Domalik-pyzik, J. Chłopek, K. Pielichowska, (Ed: M. I. H. Mondal), Springer International Publishing, Cham **2019**, pp. 1665–1693.

[18] J. M. Vaz, D. Pezzoli, Chevallier, C. S. Campelo, G. Candiani, D. Mantovani, *Curr. Pharm. Des.* **2018**, *24*, 866.

[19] S. Bauer, Schmuki, K. Von Der Mark, J. Park, *Prog. Mater. Sci.* **2013**, *58*, 261.

[20] F. Šulek, I. Milošev, *EUT Edizioni Università di Trieste* **2020**.

[21] B. Venkatraja, V. V. Malathy, B. Elayarajah, R. Rajendran, R. Rammohan, *Pak. J. Biol. Sci.* **2013**, *16*, 1438.

[22] B. L. Wang, J. L. Wang, D. D. Li, K.e-F. Ren, J. Ji, *Appl. Surf. Sci.* **2012**, *258*, 7801.

[23] S. Sutha, K. Kavitha, G. Karunakaran, V. Rajendran, *Mater. Sci. Eng. C* **2013**, *33*, 4046.

[24] L. Richert, Lavalle, E. Payan, X. Z. Shu, G. D. Prestwich, J. F. Stoltz, Schaaf, J. C. Voegel, C. Picart, *Langmuir* **2004**, *20*, 448.

[25] S. Wang, J. Sha, W. Wang, C. Qin, W. Li, C. Qin, *Carbohydr. Polym.* **2018**, *195*, 39.

[26] J. Borges, J. F. Mano, *Chem. Rev.* **2014**, *114*, 8883.

[27] J. M. Goddard, J. H. Hotchkiss, *Prog. Polym. Sci.* **2007**, *32*, 698.

[28] T. S. Demina, M. S. Piskarev, O. A. Romanova, A. K. Gatin, B. R. Senatulin, E. A. Skryleva, T. M. Zharikova, A. B. Gilman, A. A. Kuznetsov, T. A. Akopova, *Materials (Basel)* **2020**, *13*, 508.

[29] T. Tkavc, I. Petrinič, T. Luxbacher, A. Vesel, T. Ristić, L. F. Zemljič, *Int. J. Adhes. Adhes.* **2014**, *48*, 168.

[30] O. B. G. Assis, J. H. Hotchkiss, *Packag. Technol. Sci.* **2007**, *20*, 293.

[31] N. Ardila, Z. Ajji, M. C. Heuzey, A. Ajji, *J. Aerosol Sci.* **2018**, *126*, 85.

[32] E. Avcu, F. E. Baştan, H. Z. Abdullah, M. A. U.r Rehman, Y. Y. Avcu, A. R. Boccaccini, *Prog. Mater. Sci.* **2019**, *103*, 69.

[33] T. S. Demina, M. Y. u. Yablokov, A. B. Gilman, A. I. Gaidar, T. A. Akopova, A. N. Zelenetskii, *High Energy Chem.* **2015**, *49*, 213.

[34] M. Song, X. Lin, Z. Peng, S. Xu, L. Jin, X. Zheng, H. Luo, *Front. Mater.* **2021**, *7*, 583739.

[35] J. Narayanamoorthy, K. Tsioris, F. G. Omenetto, J. Hopwood, *Plasma Process. Polym.* **2013**, *10*, 451.

[36] S. Pradhan, V. K. Yadavalli, *ACS Appl. Electron. Mater.* **2021**, *3*, 21.

[37] D. T. Vo, C. K. Lee, *Carbohydr. Polym.* **2017**, *164*, 109.

[38] J. M. Karp, Y. Yeo, W. Geng, C. Cannizzaro, K. Yan, D. S. Kohane, G. Vunjak-Novakovic, R. S. Langer, M. Radisic, *Biomaterials* **2006**, *27*, 4755.

[39] S. Suzuki, Y. Teramoto, *Biomacromolecules* **2017**, *18*, 1993.

[40] H. Dong, H. Liu, N. Zhou, Q. Li, G. Yang, L. Chen, Y. Mou, *Coatings* **2020**, *10*, 1012.

[41] S. Lavenus, J. C. Ricquier, G. Louarn, Layrolle, *Nanomedicine* **2010**, *5*, 937.

[42] D. Alkekhia, T. Hammond, A. Shukla, *Annu. Rev. Biomed. Eng.* **2020**, *22*, 1.

[43] A. Arkhangelskiy, D. Maniglio, A. Bucciarelli, V. K. Yadavalli, A. Quaranta, *Adv. Mater. Interfaces* **2021**, *8*, 2100324.

[44] T. P. Nguyen, Q. V. Nguyen, V.-H. Nguyen, T.-H. Le, V. Q. N. Huynh, D.-V. N. Vo, Q. T. Trinh, S. Y. Kim, Q. V. Le, *Polymers (Basel)* **2019**, *11*, 1933.

[45] S. Guang, Y. An, F. Ke, D. Zhao, Y. Shen, H. Xu, *J. Appl. Polym. Sci.* **2015**, *132*, n/a.

[46] H. Perry, A. Gopinath, D. L. Kaplan, L. Dal Negro, F. G. Omenetto, *Adv. Mater.* **2008**, *20*, 3070.

[47] R. Eivazzadeh-Keihan, F. Radinekiyan, H. A. M. Aliabadi, S. Sukhtezari, B. Tahmasebi, A. Maleki, H. Madanchi, *Sci. Rep.* **2021**, *11*, 1.

[48] J. Park, S. G. Lee, B. Marelli, M. Lee, T. Kim, H. K. Oh, H. Jeon, F. G. Omenetto, S. Kim, *RSC Adv.* **2016**, *6*, 39330.

[49] A. Maziz, O. Leprette, L. Boyer, C. Blatché, C. Bergaud, *Biomed. Phys. Eng. Express* **2018**, *4*, 065012.

[50] H.u Tao, B. Marelli, M. Yang, B.o An, M. S. Onses, J. A. Rogers, D. L. Kaplan, F. G. Omenetto, *Adv. Mater.* **2015**, *27*, 4273.

[51] M. Narimisa, F. Krčma, Y. Onyshchenko, Z. Kozáková, R. Morent, N. De Geyter, *Polymers (Basel)* **2020**, *12*, 354.

[52] S. Banerjee, E.k Adhikari, Sapkota, A. Sebastian, S. Ptasinska, *Materials (Basel)* **2020**, *13*, 2931.

[53] J. Kredl, J. Kolb, U. Schnabel, M. Polak, K. D. Weltmann, K. Fricke, *Materials(Basel)* **2016**, *9*, 274.

[54] A. Michelmore, Martinek, V. Sah, R. D. Short, K. Vasilev, *Plasma Processes Polym.* **2011**, *8*, 367.

[55] F. Arefi, V. Andre, Montazer-Rahmati, J. Amouroux, *Pure Appl. Chem.* **1992**, *64*, 715.

[56] N. V. Bhat, D. S. Wavhal, *Sep. Sci. Technol.* **2000**, *35*, 227.

[57] M. Macgregor, K. Vasilev, *Materials (Basel)* **2019**, *12*, 191.

[58] M. Davoodbasha, S. Y. Lee, J. W. Kim, *Int. J. Biol. Macromol.* **2018**, *118*, 1511.

[59] T. Vasilieva, A. Sigarev, D. Kosyakov, N. Ul'yanovskii, E. Anikeenko, D. Chuhchin, A. Ladesov, A. M. Hein, V. Miasnikov, *Carbohydr. Polym.* **2017**, *163*, 54.

[60] D. Sun, J. Turner, N. Jiang, S. Zhu, L. Zhang, B. Falzon, C. McCoy, P. Maguire, D. Mariotti, D. Sun, *Matter. Sci.* **2019**, 10.26434/chemrxiv.9849806.v1.

[61] Z. Wang, M. Xing, O. Ojo, *RSC Adv.* **2014**, *4*, 55790.

[62] C. Mao, J. J. Zhu, Y. F. Hu, Q. Q. Ma, Y. Z. Qiu, A. P. Zhu, W. B. Zhao, J. Shen, *Colloids Surf. B* **2004**, *38*, 47.

[63] M. Kanchana, R. M. Jayappriyan, B. Kumar, A. Usha, *J. Polym. Mater.* **2017**, *34*, 747.

[64] A. G. Moutzouri, G. M. Athanassiou, *Ann. Biomed. Eng.* **2011**, *39*, 730.

[65] G. A. T. da Silveira, J. B. M. Rocha Neto, J. Kerwald, H. F. Carvalho, M. M. Beppu, *Med. Devices Sens.* **2021**, *4*, e10142.

[66] M. Bračič, T. Mohan, T. Griesser, K. Stana-Kleinschek, S. Strnad, L. Fras-Zemljič, *Adv. Mater. Interfaces* **2017**, *4*, 1700416.

[67] Y.u-C. Wu, T. M. Lee, J. C. Lin, S.-Y.u Shaw, C.-Y.u Yang, *J. Biomater. Sci., Polym. Ed.* **2010**, *21*, 563.

[68] R. Molina, Jovancic, S. Vilchez, T. Tzanov, C. Solans, *Carbohydr. Polym.* **2014**, *103*, 472.

[69] K. Kyzioł, J. Rajczyk, K. Wolski, A. Kyzioł, B. Handke, Ł. Kaczmarek, Z. Grzesik, *Mater. Sci. Eng. C* **2021**, *121*, 111848.

[70] S. Seuss, M. Lehmann, A. Boccaccini, *Int. J. Mol. Sci.* **2014**, *15*, 12231.

[71] A. Matica, G. Menghiu, V. Ostafe, *New Front. Chem.* **2017**, *26*, 75.

[72] L. Figueiredo, C. Moura, L. F. V. Pinto, F. C. Ferreira, A. Rodrigues, *Procedia Eng.* **2015**, *110*, 175.

[73] Q. Lu, X. Hu, X. Wang, J. A. Kluge, S. Lu, Cebe, D. L. Kaplan, *Acta Biomater.* **2010**, *6*, 1380.

[74] E. S. Wahyuni, F. Arifan, in *E3S Web of Conf., EDP Sciences* **2018**, p. 3012.

[75] X. Wang, H. J. Kim, Xu, A. Matsumoto, D. L. Kaplan, *Langmuir* **2005**, *21*, 11335.

[76] F. Cleymand, H. Zhang, G. Dostert, Menu, E. Arab-Tehrany, E. Velot, J. F. Mano, *RSC Adv.* **2016**, *6*, 83626.

[77] Y. Qi, H. Wang, K. Wei, Y. Yang, R.-Y. Zheng, I. Kim, K.-Q. Zhang, *Int. J. Mol. Sci.* **2017**, *18*, 237.

[78] C. C. Chen, S. Riou, S. L. Hsu, H. D. Stidham, *Langmuir* **1996**, *12*, 1035.

[79] W. M. Saltzman, T. R. Kyriakides, *Cell Interactions with Polymers*, Fourth Ed. Elsevier, Amsterdam, New York **2013**.

[80] D. N. Rockwood, R. C. Preda, T. Yücel, X. Wang, M. L. Lovett, D. L. Kaplan, *Nat. Protoc.* **2011**, *6*, 1612.

[81] A. Patelli, F. Mussano, Brun, T. Genova, E. Ambrosi, N. Michieli, G. Mattei, Scopece, L. Moroni, *ACS Appl. Mater. Interfaces* **2018**, *10*, 39512.

[82] A. Bucciarelli, T. Muthukumar, J. S. Kim, W. K. Kim, A. Quaranta, D. Maniglio, G. Khang, A. Motta, *ACS Biomater. Sci. Eng.* **2019**, *5*, 6374.

[83] A. Bucciarelli, S. Chiera, A. Quaranta, V. K. Yadavalli, A. Motta, D. Maniglio, *Adv. Funct. Mater.* **2019**, *1901134*, 1901134.

[84] P. B. Tooke, *Trends Anal. Chem.* **1988**, *7*, 130.